Volume 1 | Number 1 | Jan 2013 | Pages 1–100

Green Chemistry

Cutting-edge research for a greener sustainable future

www.rsc.org/greenchem

Stille couplings in water @RT

ROYAL SOCIETY OF CHEMISTRY

ROYAL SOCIETY OF CHEMISTRY

www.rsc.org/greenchem

1   **Interfacial improvements in biocomposites based on poly(3-hydroxybutyrate) and poly(3-**

2   **hydroxybutyrate-*co*-3-hydroxyvalerate) bioplastics reinforced and grafted with *α*-cellulose**

3   **fibers**

4   Liqing Wei [a], Nicole M. Stark [b], and Armando G. McDonald [a,*]

5   [a] Renewable Materials Program, Department of Forest, Rangeland and Fire Sciences, University

6   of Idaho, Moscow, Idaho 83844-1132, United States

7   [b] U.S. Department of Agriculture, Forest Service, Forest Products Laboratory, One Gifford

8   Pinchot Drive, Madison, Wisconsin 53726-2398, United States

9   [*] Corresponding author. Tel.: +1 (208) 885 9454; Fax: +1 (208) 885 6226; E-mail address:

10   armandm@uidaho.edu

11

Table of contents
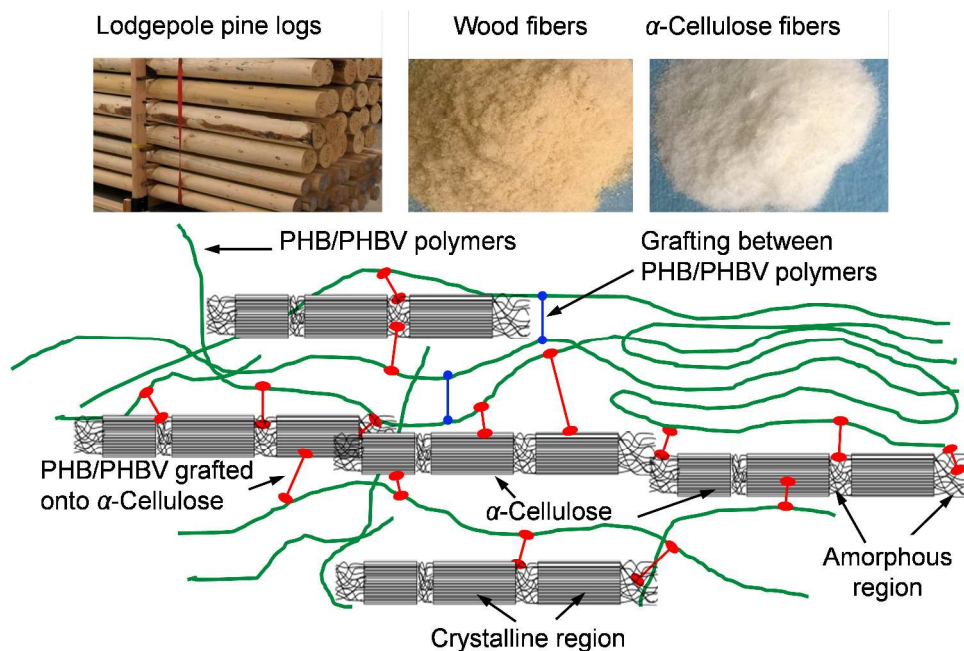
13
14   This in-situ grafting modification offers an effective approach to improve the properties of

15   biocomposite materials from sustainable resources.

Abstract

In this study, α-cellulose fibers reinforced green biocomposites based on polyhydroxybutyrate (PHB) and the copolymer poly(3-hydroxybutyrate-*co*-3-hydroxyvalerate) (PHBV) were prepared and characterized. The α-cellulose fibers were isolated from at-risk intermountain lodgepole pine wood by successive removing of extractives, lignin and hemicellulose. Grafting of PHB or PHBV onto cellulose was conducted using reactive extrusion with dicumyl peroxide free radical initiation at high temperature. It is postulated that the grafted copolymers at the interfaces of cellulose and polymer matrix performed as interfacial coupling agent. Grafting tended to interact with both the hydrophilic fibers and hydrophobic PHB or PHBV matrix. The biocomposites were characterized by scanning electron microscopy (SEM) and dynamic mechanical analysis (DMA) and indicated good interfacial bonding and compatibility between the two phases. The mechanical properties of the biocomposites were improved by grafting due to improved stress transfer between the two interphases of fiber/polymer matrix as compared to the blend control composite. The crystallinity of PHB, PHBV and cellulose in the biocomposite were reduced as determined by Fourier transform infrared spectroscopy (FTIR), wide-angle X-ray diffraction (WAXD), and differential scanning calorimetry (DSC) analyses. This *in-situ* reactive extrusion process offers an effective approach to improve the properties of biocomposite materials from sustainable resources.

1. Introduction

Strong, lightweight, and moldable plastics are used in thousands of products that improve the quality and bring convenience to our everyday lives. However, at least 40% of these conventional (petroleum-based) plastics are used in short-term applications (e.g. throwaway

39   cups, utensils, plastic bags) and after being disposed the resulting waste can quickly lead to both

40   terrestrial and marine environmental pollution.[1, 2] In brief, petroleum-based plastics are not

41   sustainable, which drives the efforts to develop more environmentally benign plastics and

42   materials. Some of the most commonly known bio-based and biodegradable plastics from

43   renewable resources include polylactic acid (PLA), polyhydroxyalkanoates [PHAs, e.g.

44   polyhydroxybutyrate (PHB) and poly(hdyroxybutyrate-co-hydroxyvalerate) (PHBV)],

45   thermoplastic starch, protein based plastics and the most abundant terrestial polymer on earth,

46   cellulose and its derivatives.[3, 4] Extensive application of these bioplastics, notably PHB and

47   PHBV, will occur only after overcoming challenges including poor melt elasticity, low thermal

48   degradation temperature, high crystallinity leading to brittleness for PHB, and low crystallization

49   rate of PHBV.[5, 6] These features, especially low melt elasticity, limit their processibility window,

50   for example, during extrusion processes typically used for film, injection molding, blown-film

51   manufacture, thermoforming, and fiber spinning.[5, 7]

52   Another critical issue is the millions of acres of forestland that have become prone to

53   disease and insect attack in the Inland-Northwest of the United State, and high risk for

54   catastrophic wildfire because of overstocked stands.[8] Approximately 6 million dry tons of sound

55   dead wood from Idaho's National Forests is available. Of this, a sustainable level of over one

56   million dry tons/year of logging residues and thinnings are potentially available for producing a

57   variety of bioproducts. Therefore, there is a need to generate materials, such as cellulose, from

58   this abundant woody biomass for use in value-added products.

59   Wood fibers have been used as fillers in thermoplastics to produce wood plastic composites

60   (WPCs), which can be used in various applications (decks, railings and automotive) due to their

61   well acceptable properties, low costs, and renewability.[9] WPC performances can be further

62 improved by exchanging wood fiber for cellulose fiber based on its improved thermal stability

63 and mechanical properties. The cellulose fibers have been widely used as reinforcing filler into

64 conventional thermoplastics, such as polypropylene and polyethylene.[10-13] Some mechanical

65 properties, such as Young's modulus and tensile strength, were improved due to the addition of

66 cellulose fibers.[12] However, the presence of a large number of hydroxyl groups results in a polar

67 fiber surface; it is very difficult to disperse polar cellulose in a non-polar polymer matrix. This

68 difficulty can result in poor interfacial bonding between the cellulose and thepolymer matrix.

69 Poor adhesion at the interface means that the full capabilities of the composite cannot be

70 exploited and leads to low mechanical properties and a reduced life span.[11] Due to this reason,

71 cellulose performs as simple filler not a true reinforcing agent. Research to improve the

72 interfacial adhesion of biocomposites continues. Extensive studies have been conducted using

73 coupling agents (e.g. maleated-polypropylene and maleated-polyethylene) to enhance the

74 interfacial adhesion of fiber filler and polymer matrix.[14] Other efforts including

75 chemical/physical treatments of fiber fillers to reduce the hydrophilicity of cellulose fiber

76 surfaces have gained much more attention.[15-18] Although these modifications result in a decrease

77 in moisture absorption and an increase in mechanical properties, biodurability and

78 weatherability, the processes used for cellulose modification are costly and involve toxic

79 chemicals which could be a deterrent to its use.[9, 19]

80 　　By exchanging conventional plastics (e.g. polyethylene and polypropylene) with bioplastics

81 (e.g. PHB and PHBV), which are less hydrophobic, will produce a fully bio-based composite

82 material that is sustainably derived with good mechanical properties (flexural/tensile strength

83 and stiffness) and biodegradation behaviors.[17, 20-22] Additionally, biocomposite properties can be

84 improved by incorporating modified cellulose fibers into a bioplastic matrix.[23-25] Recently, the

85   reaction mechanism of a "grafting onto" method has been successfully studied by grafting PHB

86   polymer onto cellulose fibers through the reactive extrusion processing with the use of small

87   amount of peroxide (Fig. 1).[26] When the peroxide is exposed to heat during extrusion it will

88   decompose into strong free radicals which tend to abstract H's from the polymer and cellulose

89   molecular chains and initiate the grafting between the two phases in composites. Via the strategy

90   of grafting PHB or PHBV onto cellulose this will retain the stiffness of cellulose and the

91   flexibility of the polymer matrix (PHBV especially). In addition, the use of reactive extrusion

92   which limits the use of solvents and the treatment of cellulose, which makes it a valuable

93   alternative to improve the performances of cellulose reinforced bioplastics composites.

94   Chemically coupling PHB to cellulose fiber provides excellent stress transfer and hydrophobic-

95   hydrophilic compatibility between the two phases in the biocomposite material with no external

96   non-biodegradable coupling agent or compatibilizers are employed. This in-line modification

97   process can be applied easily to industrial scale production of biocomposites.

98   Our aim in this study was to isolate α-cellulose (αCell) fibers from in-risk lodgepole pine

99   wood. The "grafting onto" strategy was used to prepare cellulose-graft-PHBV (αCell-g-PHBV)

100   or αCell-g-PHB biocomposites with improved properties due to enhanced interfacial adhesion.

101   The surface morphology, chemistry, and crystalline structure of the modified biocomposites

102   were characterized by microscopy, Fourier transform infrared spectroscopy (FTIR) spectroscopy,

103   and wide angle X-ray diffraction (WAXD), respectively. Tensile tests were conducted on the

104   injection molded dog-bone specimens. Thermal properties, such as thermal transition and

105   crystallinity, thermal degradation, dynamic flexural properties, and thermal mechanical

106   properties of biocomposites were assessed by thermal analysis.

107

2. Results and discussion

2.1. *α*-Cellulose fiber analysis

The chemical composition of the original wood and *α*Cell fibers for CH_2Cl_2 extractive, lignin, and carbohydrate content/composition was determined and shown in Table 1.[27] Lodgepole pine wood was comprised of 39% cellulose. After isolation, *α*Cell had a 96% purity based on glucose content.

The *α*Cell fiber size (weight) distribution was determined using an automatic vibratory sieve shaker. As shown in Table 2, the major part of the *α*Cell fiber was smaller than 250 μm, with 65% of the fibers were between 70 and 177 μm. Further information concerning *α*Cell fiber size (length and diameter) was achieved by optical microscopy. The micrographs of each screened fraction are shown in Fig. 2. Single fibers were observed (rod like), especially for the fractions that were > 60 mesh (Fig. 2c, 2d, 2e and 2f). The length (L) and diameter (d) of these fibers fractions were measured and averaged from 200 fibers. The weight normalized fiber L and d were 0.5 mm and 15.1 μm, respectively. The L of the >80, >100, and >200 mesh classified fibers ranged between 0.6 and 0.8 mm, while the d of these fractions were comparable around 19 μm. The fines fraction (<200 mesh) had a much smaller L (0.4 mm) and d (14 μm) than the coarser fractions. The 40 and 60 mesh fractions comprised of fiber bundles (Fig. 2a and 2b); hence the fiber length and diameter were difficult to be determined. As shown in Table 2, 59% (weight fraction) of the *α*Cell fibers had an aspect ratio (L/d) of 31 and is considered microcrystalline.[28] The aspect ratio was shown to decrease with a finer mesh size.

2.2. Reaction conditions optimization and grafting efficiency

The effect of two factors (DCP concentration: 2-5 %; reaction time, t_R: 5-15 min) was

131   investigated to optimize the grafting efficiency between αCell and PHB (or PHBV) polymer

132   matrix. The extruded composite strands were extracted with $CHCl_3$ to remove any nonreacted

133   PHB/PHBV or smaller homopolymer molecules and then filtered to remove nongrafted αCell

134   fibers (Note: CH_2Cl_2 and $CHCl_3$ used in this research were recovered for reuse to reduce

135   environmental impact). The dry weight of the copolymer gels was recorded and gel% was

136   calculated with respect to the dry weight of the starting materials. The optimized total

137   concentration of DCP and t_R were 2% and 10 min, respectively, to give the maximum αCell-*g*-

138   PHB and αCell-*g*-PHBV copolymer gel% and well mixed biocomposites samples. The degree of

139   grafting efficiency (GE%, weight % of PHBV (or PHB)) grafted onto αCell backbone was

140   calculated),

141         $$GE\% = (W_{gf} - W_{\alpha Cell})/W_{PHB/PHBV} \times 100 \qquad (1)$$

142   where W_{gf}, $W_{\alpha Cell}$, and $W_{PHB/PHBV}$ are the weights of the grafted copolymer gel recovered after

143   Soxhlet extraction, initial αCell, and initial PHB (or PHBV) weights, respectively.[19] The simple

144   blended composites were also extracted in the same way as grafted samples. The GE% of simple

145   blends was < 0.5%, and thus being neglected in this study. The highest GE% value of αCell with

146   PHBV was 45% but that with PHB was 35%, when biocomposites were processed under the

147   same optimized reactive conditions (DCP: 2 wt%; t_R: 10 min). As shown in Fig. 1, the grafting

148   reactions occurred at the tertiary –CH sites of PHB and PHBV. PHBV copolymer has one

149   additional tertiary –CH site in each comonomeric unit as compared with the PHB, therefore,

150   higher GE% was observed for αCell-*g*-PHBV copolymers. It is worth noting that the high GE%

151   can also be ascribed to partial crosslinking/grafting of the polymer matrices (Fig. 1a).

152

153   **2.3. Surface morphology of biocomposites**

154   The SEM micrographs of the biocomposites surfaces are shown in Fig. 3. The grafted

155   biocomposites (Fig. 3b and 3d) showed a continuous interphase between fiber and polymer

156   matrix, indicating that the polymer was grafted onto αCell by peroxide initiation. In contrast,

157   blends of αCell-PHB and αCell-PHBV showed discrete zones of PHB or PHBV and αCell fibers

158   (Fig. 3a and 3c), and the fibers were easily pulled out from the matrix when microtomed. A

159   similar trend was observed with peroxide treated sisal fibers filled in polyethylene composites

160   system.[29] An improved compatibility between αCell and the polymer matrix was obtained due to

161   peroxide induced grafting (Fig. 3b and 3d)**.** It was therefore postulated that the grafted copolymer

162   formed on the interfaces of αCell and PHBV (or PHB) coupled the hydrophilic αCell to the

163   hydrophobic PHBV (or PHB) matrix (Fig. 1). Micrographs at magnification of 200x (Fig. 3e to

164   3h) showed the cellulose fibers have been separated during the mixing extrusion process are well

165   dispersed in the polymer matrices, especially in the grafted composites as compared to the

166   simple blends. On average a random orientation of cellulose fibers into the polymer matrices for

167   both grafting as well as their simple blends was observed. However, the surfaces of αCell fibers

168   became rougher and more amorphous due to peroxide treatment, which may provide higher

169   possibility of access for melted polymers to attach onto during composites processing. This

170   further suggested better interfacial adhesion between αCell fibers and PHB (or PHBV) due to

171   grafting.

172

173   **2.4. Characterization of biocomposites by FTIR and XRD**

174   The crystalline nature of PHB and its composites materials significantly affect their

175   mechanical properties and processability as well. Copolymerization of 3-hydroxybutyrate with

176   other monomeric units, such as 3-hydroxyvalerate (3HV), to form PHBV copolymers has been

8

177   proven to be one of the most effective strategies to reduce the crystallinity of PHB. These

178   copolymers showed improved mechanical properties as a result of being less crystalline, which is

179   contributed to the presence of dislocations, crystal strain and smaller crystallite sizes due to the

180   disruption of 3HV unit to PHB crystal lattice.[30] The degree of crystallinity of PHB and PHBV

181   can be obtained by a combination of FTIR and WAXD analyses. Fig. 4a showed the FTIR

182   spectrum of the composites samples with characteristic absorbance peaks arising from αCell and

183   PHBV (or PHB). The absorbance bands at 980, 1230, 1720 cm^{-1} were assigned to the crystalline

184   regions of PHB or PHBV polymers, and as expected the intensities of these peaks were lower for

185   PHBV based samples than those of PHB's. This further indicated that the copolymer PHBV was

186   less crystalline than PHB. It was shown that the intensities of these crystalline bands for the

187   grafted composites were reduced significantly, due to grafting, compared to their simple blends

188   (αCell-PHB and αCell-PHBV). The shoulder at 1740 cm^{-1} of the band centered at 1720 cm^{-1} was

189   assigned to the carbonyl (C=O stretching) group from the amorphous region of PHB and PHBV,

190   and it became more intense after grafting (see the peak fitting of C=O region showing in Fig. 4c).

191   This observation suggested that successful grafting between the matrix (PHB and PHBV) and

192   αCell reinforcement was achieved, which would hinder the crystallization of PHBV (or PHB)

193   macromolecular chains from melts, resulting in a higher proportion of amorphous PHBV (or

194   PHB). It is worth noting that the reduction of crystallinity of grafted composites could also be

195   attributed to the crosslinking of polymer matrix (PHB-PHB or PHBV-PHBV). In addition, due to

196   the high degree of crystallinity/rigidity with the less mobile cellulose, only radicals formed on its

197   surfaces of the crystalline and amorphous regions would be more accessible to the molten

198   PHB/PHBV (with radicals) which would then be able to form grafts in the composites.

199   Therefore, the band at 1429 cm^{-1} (symmetric –CH$_2$ bending), a characteristic of amorphous

200　cellulose, which appeared in the grafted composites, again providing further evidence that

201　grafting had occurred. To further confirm that the crystallinity was reduced due to grafting,

202　quantitative analyses of the spectra for PHBV (and PHB) and cellulose crystallinity were

203　performed. The spectral ratio of 1370/2900 cm^{-1} bands (total crystallinity index, TCI, Equation

204　3) was shown to be proportional to the crystallinity degree of cellulose, while the band ratios

205　1720/1740 cm^{-1} (carbonyl index, $I_{C=O,PHB/PHBV}$, Equation 4) and 1230/1450 cm^{-1} (C-O index, $I_{C-O,}$

206　$_{PHB/PHBV}$, Equation 5) reflect the crystallinity of PHB or PHBV polymers. Quantitative analysis

207　of the infrared crystallinity ratios were calculated from the peak fitted spectra of the –C–H (and –

208　CH_2 stretching) at 2900 cm^{-1} (Fig. 4b), the carbonyl region (1800-1680 cm^{-1}) for PHB (Fig. 4c),

209　and –C–H bending centered and1370 cm^{-1} from crystalline region for cellulose (Fig. 4d). The

210　analyzed data for neat PHB and PHBV, αCell, αCell-PHB blend, αCell-PHBV blend, and grafted

211　composites (αCell-g-PHB and αCell-g-PHBV) are given in Table 4. The addition of αCell

212　resulted in a reduction in PHBV (and PHB) crystallinity of the blended composites slightly,

213　while grafting reduced all the three crystallinity indices significantly. The grafted copolymers

214　between αCell and PHBV (or PHB) matrix had improved compatibility, which would improve

215　the stress transfer between the two phases of hydrophilic cellulose and hydrophobic polymer.[26]

216　　　　To further investigate the effect of the grafting on the crystalline structures of PHB and

217　cellulose segments, vacuum dried samples were subjected to WAXD analysis (Fig. 5). αCell

218　showed four crystalline peaks corresponding to (101), (10-1), (002), and (040) planes showing at

219　2θ scale of 14°, 16°, 22°, and 35°, respectively. The maximum diffractogram intensity was

220　observed in the (002) plane. This is a typical pattern of cellulose I. Both PHB and PHBV

221　samples showed crystalline peaks at 2θ near to 13°, 17°, 20°, 21°, 22°, 26° and 27°, respectively,

222　ascribing to planes of (020), (110), (021), (101), (121), (040), and (200). The most intense peak

223 for PHB and the composites samples was at 17°, whereas the most intense peak for PHBV based

224 samples was observed at 13°. It is assumed that the reduced crystallinity of PHBV as compared

225 to PHB could be the main contributor to peak broadening for all the crystalline planes. Such

226 results can be explained by the reason that the presence of αCell suppressed the nucleation of

227 polymer, especially for PHBV, in the simple blends. The similar reduction of PHB and PHBV

228 crystallinity was also found in PHB/cellulose (Whatman CF1) and PHBV/PLA/PBS

229 (poly(butylene succinate)) blends, respectively.[26]

230 The Gaussian function was used for peak fitting of the WAXD diffractograms, meantime,

231 the FWHM values were obtained accordingly. Crystallinity indices were calculated from the

232 ratios of fitted peak intensities, and crystal sizes according to Scherrer's formula using a shape

233 constant K = 0.9 for PHBV (and PHB) and cellulose (Table 3). Crystallinity index[19] and average

234 crystal width were 59.1% (CrI%$_{\alpha Cell}$, Equation 6) and 250 Å (D$_{002}$) for αCell, 61% (CrI%$_{PHB}$,

235 Equation 7) and 1274 Å (D$_{020}$) for PHB, and 36.2% (CrI%$_{PHBV}$, Equation 8) and 190 Å (D$_{020}$,

236 Equation 9) for PHBV, respectively. PHBV had a much smaller crystal size and significantly

237 lower degree of crystallinity than PHB based materials. The lower crystallinity for PHBV would

238 result in a more ductile/flexible material than PHB. The large crystal size which would induce

239 inter-spherulitic cracks is one of the leading reasons for the brittleness of PHB.[31, 32] The simple

240 blending of PHB (or PHBV) with αCell was shown to reduce slightly the crystallinity indices

241 and crystal sizes of the PHB (or PHBV) polymer. Nevertheless, the decreasing trend was more

242 significant as a result of grafting (Table 3), which contributed to new C–C bonds being formed

243 which limited the numbers of PHB or PHBV molecular chains involved in crystallization

244 processes from the polymer melt. The PHB and PHBV molecular chains with more grafted sites

245 would contribute to an increase in the amorphous component due to inhibited crystallization.

246 These results were consistent with the findings from infrared crystallinity indices results and

247 supported the lowering in crystallinity of the polymer matrix by grafting. Smaller crystal sizes of

248 the grafted biocomposites were observed suggesting that the formation of large crystals of either

249 PHBV (or PHB) was restricted. This could be one of the major reasons for to the improved

250 mechanical properties of grafted biocomposites as compared to the simple blends of cellulose

251 and polymer (PHB or PHBV).

252

253 **2.5. Influence of grafting on mechanical properties of biocomposites**

254 The density (ρ) and tensile properties (strength (σ), modulus (E), elongation at break (ε),

255 and energy at break (EAB)) of molded neat bioplastics and their composites are given in Table 4.

256 The ρ of all PHB, PHBV and biocomposites samples ranged from 1.10 to 1.18 g/cm^3 and thus

257 was not a major factor causing differences in tensile properties between treatments. The density

258 of the biocomposites remains similar to neat plastics, which may be because the density of

259 cellulose fiber was about 1.5 g/cm^3 and only 20% of cellulose was used in the composites.

260 According to Maldas and Kokta,[33] the mechanical properties of short-fibers and plastic

261 composites are strongly influenced by the fiber content, fiber morphology (size and shape), the

262 orientation (random or unidirectional) of the fillers, and the fiber-polymer adhesion. The σ is

263 more dependent on the fiber-polymer interaction (compatibility) while E is dependent more on

264 fiber content and morphology (i.e. aspect ratio).[14] The grafted biocomposites resulted in an

265 increase of E and σ. The E values of αCell-PHB and αCell-PHBV biocomposites were higher

266 than those of the neat PHB and PHBV, respectively. This indicated the reinforcement effect of

267 cellulose fibers to the polymer matrices. On the other hand, the increments of E were much more

268 significantly for the grafted composites due to grafting between cellulose and polymer matrices.

269   The neat PHBV and blended αCell-PHBV composite showed lower E as compared to PHB and

270   blended αCell-PHB, which was attributed to the lower tensile properties of PHBV.[34] Whereas,

271   the grafted αCell-g-PHBV composites showed comparable E to neat PHB, suggesting the

272   reinforcement of αCell fibers was improved via grafting. Moreover, the increased E of polymer

273   matrix due to crosslinking between polymer chains (see Fig. 1) would partially contribute to the

274   E increase of grafted composites.

275   The ductility reflected by ε values was significantly higher for PHBV based composites,

276   which contributed to higher flexibility of PHBV (22% HV) than PHB homopolymers.[32] Work on

277   PHB/PHBV-flax fiber composites showed higher values of ε for PHBV based composites than

278   PHB based composites.[34] For composites made from PHB or PHBV, σ at ultimate yield point

279   was increased with the addition of αCell fibers accompanied with a decrease in ε. In comparison

280   with PHB and its composites the copolymer PHBV based composites showed a somewhat lower

281   σ, around 12 MPa. For the grafted composites (αCell-g-PHB and αCell-g-PHBV), higher E and ε

282   were obtained when compared to their simple blends. This finding suggests that grafting didn't

283   just enhance the fiber-polymer matrix interaction but also increased the ductility of the resulting

284   composite due to crosslinking between polymer chains (PHB-PHB and PHBV-PHBV). This was

285   possibly caused by a lower degree of crystallinity of cellulose and the bioplastic as discussed in

286   the previous section (Table 3). The toughness of all samples was assessed by their EAB values

287   (Table 4). Neat PHB and PHBV showed respective toughness of 0.33 and 0.45 J, indicating that

288   the PHBV copolymers had an improved toughness than PHB. EAB was also shown to increase

289   with addition of 20% αCell fibers. For example, the EAB of the simple blends, αCell-PHB and

290   αCell-PHBV, were 0.41 and 0.45 J, respectively. A similar result was obtained in a study on the

291   fracture toughness changes due to addition of 10 to 30 % wheat straw fibers into PHB matrix.[35]

292   Grafting of PHB/PHBV onto αCell improved the toughness significantly ($p < 0.05$) by 46% and

293   44%, respectively, as compared to their simple blends, αCell-PHB and αCell-PHBV.

294   According to Kelly-Tyson theory, the critical fiber length ($L_{c/\alpha Cell}$) is used to evaluate the

295   fibers performing as reinforcement or just filler to the polymer matrix. It is assumed fiber

296   morphology (length and aspect ratio) would not be influenced significantly during single screw

297   mixing/extrusion processing, for example by shearing, and thus the $L_{c/\alpha Cell}$ can be estimated as

298   follows:

299         $$L_{c/\alpha Cell} = \frac{\sigma_{\alpha Cell} \times d_{\alpha Cell}}{2\tau} \qquad\qquad (2)$$

300   where $\sigma_{\alpha Cell}$ is the αCell fiber strength, $d_{\alpha Cell}$ is the fiber diameter that was averaged based on the

301   weight fraction % ($d_{\alpha Cell} = 0.015$ mm), and τ is the interfacial bonding strength of fiber and

302   polymer matrix. $\sigma_{\alpha Cell}$ and τ values were obtained from the literature, respectively at 1.5 GPa and

303   8.8 MPa.[34] Hence, the $L_{c/\alpha Cell}$ value was calculated to be 1.2 mm. Based on the fiber distribution

304   analysis as shown in Table 2, the size of αCell fibers were lower than the estimated critical

305   length required to give an adequate stress transfer between fiber and PHB (or PHBV) polymer

306   matrix. This again explained the low σ of simple blended composites without grafting. However,

307   the grafted composites (αCell-g-PHB and αCell-g-PHBV) showed improved tensile properties

308   due to better stress transfer caused by the newly formed bonds (Fig. 1) between the fiber and

309   polymer.

310

311   **2.6. Thermal properties of the bioplastics and biocomposites**

312   2.6.1. Thermal degradation behavior

313   Thermal degradation for neat PHB and PHBV and biocomposites was investigated by

314   thermogravimetric analysis (TGA) and the degradation temperatures are given in Table 5. Neat

315   PHB and PHBV started (T_{onset}) to degrade at 263 and 250 ˚C, and completed degradation (T_{comp})

316   at 303 and 292 ˚C, respectively. The HV units in PHBV did not improve the thermal stability of

317   the polymer, which agrees to previous research.[36] Degradation (98% mass loss) occurred in one

318   step for the neat polymers. This was ascribed to chain scission and hydrolysis mechanisms of

319   PHB and PHBV, resulting in a lower molar mass fragments and the formation of crotonic acid.[36]

320   All the biocomposite samples showed two degradation stages, of which the first stage was

321   ascribed to the PHB/PHBV degradation while the second stage was from αCell degradation. The

322   T_{onset} for the αCell-PHB and αCell-PHBV blends was close to neat PHB/PHBV, and 80% of the

323   biocomposite samples degraded in the first stage, aligning to the formulation (αCell:PHB = 1:4;

324   αCell:PHBV = 1:4). These data indicated that simple blending of αCell fibers with PHB/PHBV

325   did not improve the thermal stability of the polymer matrix. These results are consistent with

326   findings for PHB and cotton fiber blends.[26] However, the grafted biocomposites (αCell-g-PHB

327   and αCell-g-PHBV) had a higher T_{onset} by > 10 ˚C than neat PHB and PHBV. The temperature of

328   maximum decomposition rate (T_{max}) in the first stage for sample αCell-g-PHB was > 10 ˚C

329   higher than T_{max} of neat PHB (285 ˚C). Furthermore, the T_{max} in the second stage due to αCell

330   ($T_{\alpha Cell}$) component degradation was also increased compared to αCell-PHB blends. Similar

331   results were obtained for PHBV based biocomposites. Grafting modification improved the

332   thermal stability for both the reinforcement (αCell) and the polymer matrix (PHB and PHBV).

333   Grafting between αCell and polymer matrix and a small amount of cross-linked PHB or PHBV

334   resulted in forming more C–C bonds (Fig. 1b and 1c), which would require more energy/thermal

335   input to decompose the resultant grafted biocomposites.

336

337   2.6.2. Different scanning calorimetry (DSC) analysis

338   The thermal events of glass, crystallization, melting transitions of neat PHB/PHBV, simple

339   blends, and grafted biocomposites were studied using DSC. Fig. 6 shows the DSC thermograms

340   for neat PHB and PHBV, and their biocomposites in the temperature range of -30 to 180 ˚C.

341   Thermal transitions as well as the degree of crystallinity (X_c %, Equation 10) of the materials are

342   given in Table 6. Neat PHB showed a glass transition (T_g = 4.9 ˚C) and double endothermic

343   peaks (T_{m1} = 159 ˚C and T_{m2} = 169 ˚C, labeled from low to high temperatures) corresponding to

344   melting points in the second heating scan (Fig. 6). The addition of 20 wt% αCell to neat PHB

345   (αCell-PHB blend) resulted in a slight increase in T_g (5.3 ˚C), while the grafted αCell-g-PHB

346   biocomposites increased T_g by 2 ˚C. The X_c % of αCell-PHB and αCell-g-PHB biocomposites

347   was reduced by 2.4 % and 10.4 %, respectively, as compared to neat PHB (53.4%). The

348   reduction in crystallinity (or amorphous phase increase) observed by DSC agreed with results of

349   FTIR and WAXD analyses (Table 4).

350   The T_g is directly associated with the macromolecular mobility of polymer chains, hence, a

351   lower X_c % will require less energy to move the polymer chains in the amorphous phase.

352   Therefore, a lower T_g is expected to transit the polymer from a glassy to a rubbery state if only

353   polymer matrix itself was modified by DCP as reported in our previous studies.[37] However,

354   higher T_g was observed for αCell-PHB and αCell-g-PHB biocomposites, which was possibly due

355   to the limited polymer molecular chain mobility from the rigid αCell fibers. Bhardwaj et al.[38]

356   found the similar trend for T_g of recycled fibers reinforced PHBV composites. In αCell-g-PHB,

357   extra C–C bonds due to grafting between the fibers and polymer matrix would provide further

358   restrictions in the polymer chain mobility as compared to αCell-PHB, and hence T_g was shifted

359   to a higher temperature.

360   During DSC analysis, the melt peaks, T_{m1} and $T_{m2,}$ of αCell-PHB were increased slightly

361   from 159 to 161 ˚C and from 169 to 171 ˚C, respectively, as compared to neat PHB. While the

362   αCell-g-PHB composites showed T_{m1} and T_{m2} values respectively at 155 and 164 ˚C. This

363   reduction is likely caused by the broadening molar mass distribution of the polymer matrix due

364   to grafting/cross-linking between polymer chains. A similar trend was observed for T_g, T_m's and

365   X_c % for PHBV and its biocomposites samples (Table 6). However, a more apparent change was

366   seen in the grafted αCell-g-PHBV material. This could be contributed to the chemical structure

367   of PHBV/PHB polymers[26] and the higher GE% of PHBV.

368   DSC can easily detect the significant heat release accompanying the exothermic

369   crystallization process of PHB and PHBV. The T_c is an important thermal parameter to describe

370   the crystallization behavior of fiber and plastic composites (Fig. 6 and Table 6). A sharp

371   crystallization peak was observed for all PHB-based samples and neat PHBV in the cooling scan.

372   An increase in T_c was observed when αCell fibers were incorporated into the PHB matrix (T_c =

373   85 ˚C). This suggested that the αCell fibers induced nucleation of PHB and initiated the

374   crystallization at higher temperature (i.e. > 121 ˚C) from melt. Grafting resulted in a decrease in

375   T_c (103 ˚C) of αCell-g-PHB as compared to the blended αCell-PHB material. The corresponding

376   enthalpy (ΔH_c) of αCell-g-PHB during crystallization was reduced by 12 % due to grafting. This

377   reduction was most likely due to the lower X_c % of PHBV (or PHB) in the grafted biocomposites

378   (Table 6). The exothermic peak of neat PHBV was broader than PHB, which indicated

379   nucleation and crystal growth were much slower in PHBV. This finding agrees with the

380   literature.[39] The T_c of PHBV in αCell-PHBV was reduced significantly by 28 ˚C as compared to

381   that of neat PHBV. This indicated that the addition of fibers resulted in a slower diffusion and

382   migration of PHBV copolymer chains to the surface of the nucleation point, thus decreasing T_c

383   during cooling of the αCell-PHBV melt. For the grafted biocomposites, αCell-g-PHBV, no

17

384 exothermic crystallization peak (T_c) was observed by DSC in the cooling scan. The reduction in

385 the X_c %, T_m's, and T_c was in agreement with the results reported in the case of poly(ε-

386 caprolactone) (PCL) reinforced with PCL diol grafted cellulose nanocrystals using toluene 2,4-

387 diisocyanate as coupling agent.[40] In addition, an exothermal (cold crystallization) peak (T_{cc}) was

388 observed in the heating scan of PHBV based composites (Fig. 6b). This peak was shifted from 56

389 ˚C to higher temperature (77 ˚C) due to grafting, indicating the delay of crystallization kinetics

390 (increased crystallization rate) with incorporation of cellulose fibers and grafting crosslinks.

391

392 2.6.3. Dynamic flexural properties

393   Dynamic mechanical analysis (DMA) was performed on PHB, PHBV and their composites

394 in three-point bending mode to determine the storage modulus (E') which determines the

395 dynamic rigidity of a material. The E' values of the samples at 30, 50 and 70 ˚C are given in

396 Table 7. The E' values (30 ˚C) of PHB increased by 33% and 60%, respectively by simple

397 addition of αCell and grafting of αCell, respectively. The αCell-PHBV and αCell-g-PHBV

398 biocomposites had also shown significantly increased E' values by 88 and 127%, respectively, as

399 compared to neat PHBV. PHB had a higher E' due to its high brittleness than PHBV. The higher

400 E' values for the grafted composites could be contributed to an improved compatibility and

401 dispersion of αCell fibers in the PHB/PHBV matrix as compared to their blends (αCell-PHB and

402 αCell-PHBV). Better stress transfer between the αCell and PHB/PHBV interfaces of the grafted

403 composites would also improve the rigidity of either PHB or PHBV composites.

404   The loss tangents (tan$δ$) of the various samples at 30, 50 and 70 ˚C are given in Table 7 as

405 well. Tan$δ$ values were shown to have a minimum at 50 ˚C. For both PHB and PHBV based

406 composites their tan$δ$ values were less than their matrix, especially < 30 ˚C. According to our

407   previous findings of the fiber-matrix interfacial bonding,[9, 25] the reduction of tanδ could indicate

408   better interfacial adhesion of these two phases in grafted biocomposites as compared to their

409   simple blends without being grafting modified.

410   The interfacial bonding between wood fiber and polyethylene matrix was successfully

411   evaluated by the adhesion factor (A) (Equation 11).[9] A values derived from DMA data at 30 ˚C

412   are given in Table 7. Lower A values of the grafted composites was an indicator of improved

413   interfacial interaction between the two phases, αCell and PHB or PHBV, as compared to their

414   blend. These data provided supportive evidence that an improved interaction was achieved by

415   grafting.

416

417   **2.7. Dynamic rheological properties**

418   The polymer melt properties of the biocomposites were determined by dynamic parallel

419   plate rheometry. Fig. 7 shows the dynamic elastics and viscous moduli (G' and G") of PHB

420   (175 ˚C) and PHBV (170 ˚C) based materials under isothermal conditions. For the PHB based

421   composites both G' and G" were shown to increase with frequency (ω, rad/s). At lower ω, G" was

422   higher than G' for PHB and the simple blended composite (αCell-PHB). This indicated that these

423   samples were more liquid-like, although the incorporation of αCell made the resulting

424   composites slightly more elastic which was reflected by the less difference between G" and G'

425   values. However, grafting improved the G' slightly compared to the simple blends (see Fig. 7a,

426   G' > G"), suggesting the grafted PHB onto αCell showed good elastic properties. For instance, G'

427   was increased from 12 Pa (PHB) to 1000 Pa by addition of αCell and further improvement to

428   1400 Pa was obtained by grafting (αCell-g-PHB). PHBV, αCell-PHBV and αCell-g-PHBV

429   showed higher G' and G" values than PHB series which clearly showed that the PHBV

430   copolymer had relatively better melt strength. At lower frequency, i. e. ω < 10 rad/s, G' > G" was

431   observed for PHBV and its composites, suggesting the PHBV (22 mol% HV) has better melt

432   strength (higher melt viscosity) than PHB. Conflicting results were observed in other studies on

433   the PHBV with lower HV content (12 mol%).[41] In addition, due to relatively longer chain of HV

434   as compared to HB more degrees of chain entanglements in PHBV would be presented as

435   compared to PHB. Found in previous researches,[37, 42] the melt elasticity is positively proportional

436   to the molecular chain entanglement and the degree of long chain branching. Although pure

437   PHBV is a linear polymer, the presence of HV monomeric units could provide long chain

438   branching structures. Compared to pure PHB homopolymers, PHBV can be considered as a

439   branched form of PHB, and thus PHBV and its composites showed G' > G". Similar trend (G' >

440   G") was observed between the long chain branched and linear polyethylene samples.[42]

441   The polymer melt of the copolymer PHBV had better elasticity than that of PHB (Fig. 7b). The

442   addition of αCell to PHBV increased its G" by 30%. The effect of grafting of αCell onto PHBV

443   further increased G' (5-fold) and G" (7-fold) significantly as compared to the blend. The

444   improvements of PHBV properties, relative to PHB, are most likely due to the higher grafting

445   efficiency of PHBV when using the same reactive parameters.

446   The cross-over modulus (G_c = G' = G") of grafted PHB and PHBV biocomposites shifted

447   towards higher ω. The G_c was increased from 670 Pa for PHB to 1070 Pa by addition of αCell

448   and was further increased to 2300 Pa by grafting. A similar trend was also observed for the

449   PHBV composite series. The mean relaxation time (at G_c), which is the ratio of the elastic to the

450   viscous response,[43] was increased for PHB based composites whereas it was decreased for

451   PHBV based composites due to grafting. This difference might be mainly due to the higher

452   molecular weight of PHBV as well as the fraction of crosslinked polymer (PHB-PHB,

453   PHBV/PHBV) in the grafted composites. This can result in higher molar mass distribution of

454   grafted PHBV based composites than that of PHB based composites.

455   αCell-*g*-PHBV behaved like a solid with a G' of about 5 kPa. This could be partially due to

456   long chain branching between crosslinked PHBV (or PHB) chains. There was less of a

457   magnitude increase in moduli for αCell- PHB composites as compared to αCell-PHBV due to

458   grafting. This further indicated the higher grafted efficiency of PHBV based composites with

459   incorporation of same peroxide concentration. The relatively lower degree of elasticity for PHB

460   and PHBV compared with their composites was likely caused by their higher chain stiffness, and

461   this phenomenon agrees with their higher T_m values. Therefore, peroxide induced free radical

462   initiation to create crosslinks and grafting is a practical approach to improve the industrial melt

463   processability of PHB and PHBV as well as their biocomposites.

464

465   # 3. Experimental

466   **3.1. Materials**

467   Lodgepole pine (*Pinus contorta*) lumber was sourced locally (Southern Idaho, USA). The

468   lumber was chipped then Wiley-milled to pass through a 40 mesh screen. Wood fiber (500 g)

469   was extracted with acetone (3 L, 99.5%, Macron Fine Chemicals) to yield 8.0 g of extractives.

470   Air dried extractives free wood fiber (100 g batches) was treated with 3.2 L deionized water

471   containing 30 g NaClO$_2$ (99%, Tech. Grade, Ricca Chemicals, USA) and acetic acid (20 mL,

472   99.7%, Fisher ACS, USA) at 70 $^{\circ}$C for 1 h, and this was repeated four more times to a total of 6

473   h.[44] The holocellulose fibers (150 g batch) was then extracted with 17.5% NaOH (4 L) solution

474   at 20 $^{\circ}$C with constant stirring for 5 h to afford αCell fibers by removing the hemicelluloses. The

475   αCell was recovered by filtering through a polypropylene screen (100 mesh) and washed

476   exhaustively with water under vacuum. Then, 10% aqueous acetic acid (2 L) was added to the

477   αCell and left to soak for 5 min. The αCell fiber was then washed exhaustively with water (1L,

478   10-15 times) until neutral. Finally, αCell was rinsed with acetone to accelerate drying, and then

479   dried in a vacuum oven (>24 h) to <0.5% moisture content. This method yielded 55% αCell

480   based on initial dry weight of wood.

481   Poly-3-hydroxybutyrate (PHB: M_w = 290,000 g/mol) and poly(3-hydroxybutyrate-co-3-

482   hydroxyvalerate) (PHBV: 22 mol% HV content; M_w = 400,000 g/mol) powder obtained from

483   Tianan Biopolymer Inc. (Ningbo, China). These PHAs are non-nucleated grades without any

484   additives. Dicumyl peroxide (DCP: 98%) was a product of Sigma-Aldrich (USA). CH_2Cl_2 (J.T.

485   Baker, USA) was used as received.

486

487   **3.2. Biocomposites processing**

488   The PHB and PHBV based composites were prepared according to our previous work.[26]

489   Briefly, αCell, PHB and PHBV were separately coated with DCP in acetone solution (4-8

490   mg/mL) for 30 min, and then air dried followed by drying in a vacuum oven (>24 h) for prior to

491   composites processing. DCP coated PHB or PHBV (80%) and αCell (20%; moisture content was

492   < 0.5%) were dried and premixed in a beaker. The αCell-g-PHB and αCell-g-PHBV grafted

493   biocomposites were prepared in a Dynisco Lab Mixer Molder/Extruder (LMM) using the

494   reactive extrusion process and mixed (500 rpm) for time t_R and then extruded into strands (1 mm

495   Ø) or injection molded into rectangular bars (60 x 9 x 2 mm^3). Processing temperature was

496   175 $^\circ$C for PHB and 170 $^\circ$C for PHBV based materials. The grafting efficiency (GE%) was

497   evaluated by extracting the non-soluble copolymerized gel fraction using Soxhlet extraction for

498   24 h in chloroform to remove any nonreacted PHB. The extract was then filtered through a nylon

499　　screen with pore size was about 450 μm which was large enough to allow nonreacted cellulose

500　　fibers to pass through. The conditions (DCP concentration and reaction time t_R) at which

501　　maximum grafted copolymer gel yield was considered to be optimized parameters used to

502　　prepare grafting modified biocomposites.[19] Simple blends of αCell and PHB (αCell-PHB) or

503　　PHBV (αCell-PHBV) without addition of DCP were prepared as control strand and rectangular

504　　bar samples.

505

506　　**3.3. Characterization**

507　　3.3.1. α-Cellulose fiber analysis

508　　　　Sieve analysis was performed on the isolated αCell fibers (10 g) using standard test sieves

509　　(40, 60, 80, 100, 200 mesh and pan) on a Soil Test Inc. Model CL-300B shaker for 10 min, and

510　　the weight distribution was determined. The average length and diameters of the isolated αCell

511　　fibers in each fraction were averaged from two hundred fibers dyed with safranin and observed

512　　by optical microscopy (Olympus BX51 in bright field mode and images captured using an

513　　Olympus DP70 digital camera).

514　　　　The chemical composition of the original wood and αCell fibers for CH_2Cl_2 extractive,

515　　lignin (acid soluble and Klason lignin), carbohydrate (hemicellulose and cellulose), and ash

516　　compositions were determined according to the methods described in details by Liang and

517　　McDonald.[45] More specifically, the wood and αCell fibers samples (4-5 g) were Soxhlet

518　　extracted with CH_2Cl_2 (150 mL) for 16 h in accordance with ASTM D 1108-9623 and

519　　extractives were determined gravimetrically. Lignin content was determined as acid insoluble

520　　and acid soluble lignin on extractive free samples. Carbohydrate analysis was performed on the

521　　2-stage acid-hydrolyzates according to ASTM E 1758-01.26 with slight modification. The dried

522   sample (200 mg) was incubated in 72% H_2SO_4 (2 mL) for 1 h at 30 °C, then diluted into 4%

523   H_2SO_4, and subjected to secondary hydrolysis in an autoclave (117 KPa and 121 °C) for 30 min.

524   The hydrolyzate was filtered through a sintered crucible to obtain acid insoluble (Klason lignin)

525   residue content gravimetrically after oven dried at 104 °C. An aliquot of the hydrolysate (made

526   up to 250 mL) was taken to determine acid soluble lignin content at 205 nm using an absorption

527   coefficient of 110 L/g/cm on a Beckman DU640 spectrometer. To the hydrolysate (5 mL)

528   inositol (1 mL, 0.5 mg/mL) was added as an internal standard, then $PbCO_3$ (0.16 g) added to

529   remove sulfate, and centrifuged. The supernatant was deionized by passing through an ion

530   exchange resin cartridge (containing Amberlite IR-120 H^+ (0.5 mL) and Amberlite IRA35 OH^-

531   (0.5 mL)) and filtered through a 0.45 μm syringe filter (nylon, FisherScientific) into an HPLC

532   vial. Monosaccharides were quantified by HPLC using two Rezex RPM columns in series (7.8

533   mm × 30 cm, Phenomenex) at 85 °C equipped with a differential refractive index detector

534   (Waters Associates model 2414) on elution with water (0.5 mL/min). The chromatographic data

535   were analyzed using N2000 software (Science Technology Inc., China). The ash content of

536   lodgepole pine wood and isolated αCell fibers were determined by furnacing samples at 600 °C

537   according to ASTM D 1102-84.

538

539   3.3.2. Surface morphology of composites

540   Biocomposite bar samples were microtomed into 100 μm thick specimens and coated with

541   carbon and gold. The prepared samples were investigated at 500x and 200x magnifications using

542   a LEO Gemini field emission SEM operating at 4 kV under high vacuum.

543

544   3.3.3. Surface chemistry by FTIR spectroscopy

545 *α*Cell fibers, PHB, PHBV, and biocomposites samples were characterized by FTIR

546 spectroscopy using a Thermo Nicolet iS5 FTIR spectrometer (ZnSe attenuated total reflection

547 (ATR) probe (iD5)). Samples (in triplicate) were analyzed after vacuum drying. The absorbance

548 spectra were baseline corrected and averaged using software Omnic v9.0 (Thermo Scientific).

549 Total crystallinity index (TCI) of *α*Cell fibers, and the quantitative crystallinity indices of

550 carbonyl (C=O stretching) group ($I_{C=O, PHB/PHBV}$) and C-O stretching ($I_{C-O, PHB/PHBV}$) of

551 PHB/PHBV polymers before and after grafting were determined as follows:

552 $\quad$ $TCI = A_{1370}/A_{2900}$ $\qquad\qquad\qquad\qquad$ (3)

553 $\quad$ $I_{C=O, PHB/PHBV} = A_{1720}/A_{1740}$ $\qquad\qquad\qquad$ (4)

554 $\quad$ $I_{C-O, PHB/PHBV} = A_{1230}/A_{1450}$ $\qquad\qquad\qquad$ (5)

555 where A_{1370} and A_{2900} are the areas of *α*Cell peaks at 1370 and 2900 cm^{-1}, respectively, and

556 A_{1230}, A_{1450}, A_{1720} and A_{1740} are the areas of the peaks near to 1230, 1450, 1720 and 1740 cm^{-1}

557 from PHB (or PHBV) molecular chains, respectively. All band areas were obtained by peak

558 fitting processing using IGOR Pro v6 (WaveMetrics) software.[9] Gaussian functionality was

559 employed for peak fitting using selected peak width at half height (FWHM) values.

560

561 3.3.4. Crystallinity characterized by WAXD

562 The crystalline structures of *α*Cell fibers and injection molded neat PHB/PHBV and

563 biocomposites samples were characterized by WAXD (Siemens D5000 diffractometer) at room

564 temperature. The instrument was set up with a rotating Cu Kα2 X-ray tubes operating at 40 kV

565 with a current density of 30 mA. Scanning was performed over the 2θ ranging from 5 to 50$^{°}$ with

566 steps of 0.2$^{°}$. The collected diffractograms were processed and peak of interest was

567 fitted/deconvoluted (Gaussian function) using IGOR Pro v6 software. The intensity of each peak

568   identified by peak fitting was mathematically computed. The methods to determine the

569   crystallinity index of αCell (CrI$_{\alpha\text{Cell}}$), PHB (CrI$_{\text{PHB}}$),[26] and PHBV (CrI$_{\text{PHBV}}$) are according to:

570        $\text{CrI}_{\alpha\text{Cell}} = (1 - (I_{am}/I_{002})) \times 100$ (6)

571   where I_{am} is the intensity of the peak at $2\theta = 18°$ and I_{002} is the maximum intensity of the (002)

572   plane diffraction.

573   The PHB and PHBV crystallinity index was calculated according to:

574        $\text{CrI}_{\text{PHB}} = I_{17}/I_{\text{total-PHB}} \times 100$ (7)

575        $\text{CrI}_{\text{PHBV}} = I_{17}/I_{\text{total-PHBV}} \times 100$ (8)

576   where I_{17} is the intensity of the peak close to $2\theta = 17°$ and I_{total} is the total intensity of all

577   crystalline peaks of PHB ($I_{\text{total-PHB}}$) or PHBV ($I_{\text{total-PHBV}}$).

578   The crystal size dimension D_{hkl} was estimated as well by Scherrer's formula:[46]

579        $D_{hkl} = K \times \lambda / (\beta_{1/2} \times \cos\theta)$ (9)

580   where K is the crystal shape constant, λ is the X-ray wavelength ($\lambda = 0.1542$ nm, $\beta_{1/2}$ is the

581   FWHM, ≈ 2 Deg.) obtained by IGOR Pro, when peak fitting was conducted with Gaussian

582   function, and θ is the diffraction angle.

583

584   3.3.5. Tensile testing

585   All injection molded microtensile (dog-bone) samples (10 replicates) were conditioned at

586   65% relative humidity at 23 $°$C for at least 7 d. Tensile tests were performed according to ASTM

587   Standard D1708 using an Instron 5500R-1132 universal test machine with a constant strain rate

588   of 1 mm/min, 5 kN load cell, and strain measured using an extensometer (model 3542, Epsilon

589   Technology Corp.). The density of injection molded samples was calculated based on the initial

590   conditioned dry weight and dimensions.

591

592   3.3.6. Thermal analysis

593   TGA was performed on a TGA-7 (Perkin-Elmer) instrument. Samples (3-5 mg, in

594   duplicates) were heated from 50 to 900 $^{\circ}$C at a rate of 20 $^{\circ}$C/min under nitrogen (30 mL/min).

595   Data were analyzed with replicated curves were averaged using Pyris v8 software (Perkin

596   Elmer).

597   DSC measurement was performed on neat PHB/PHBV and biocomposites (4-6 mg, in

598   duplicate) using a TA Instruments model Q200 DSC with refrigerated cooling. The samples were

599   (i) equilibrated at 40 ˚C (3 min) then ramped to 190 ˚C at 10 ˚C/min, held isothermally for 5 min

600   to remove any thermal history, (ii) cooled to -50 ˚C at the rate of -10 ˚C/min and held

601   isothermally for 3 min, and (iii) reheated to 190 $^{\circ}$C at 10 $^{\circ}$C/min to record the heating scan. Data

602   were analyzed using TA Universal Analysis v4.4A software. Glass transition (T_g) and melting

603   temperatures (T_m) were determined from the peaks second heating scan, while crystallization

604   transition temperature (T_c) was obtained from the peak of cooling scan. The degree of

605   crystallinity (X_c %) of PHB and PHBV was calculated as follows:

606        $$X_c \% = \Delta H_m/(\Delta H_0 \times W_f) \times 100 \qquad\qquad (10)$$

607   where ΔH_m is the melting enthalpy of sample (PHB and PHBV polymers), and ΔH_0 is melting

608   enthalpy in J/g of 100% crystalline PHB (146 J/g),[37, 47] and W_f is the weight fraction of PHB or

609   PHBV (80%) in biocomposites samples. Note: if the differences of transition temperatures

610   between duplicates were less than 0.2 ˚C, standard deviation will not be reported.

611

612   DMA measurements were conducted on biocomposite samples using a TA Q800

613   Instruments. At least duplicate rectangular injection molded rectangular bars (60 x 9 x 2 mm^3)

614   were tested using a 3-point bending fixture (50 mm span). Samples were heated from 30 to 150

615   °C at 2 °C/min, 0.05% strain, and at a single frequency of 1 Hz. Data was analyzed by TA

616   Universal Analysis v4.4A software.

617   The αCell/PHB and αCell/PHBV interfacial adhesion was evaluated by an adhesion factor

618   (A) which was calculated from DMA results at 30 $^\circ$C as follows:[9, 48]

619       $A = (1/(1-V_f)) (\tan \delta_c/\tan \delta_m) - 1$ (11)

620   where, c and m subscripts represent biocomposites and polymer matrix (PHB and PHBV), and V_f

621   is the fiber volume fraction which was determined in accordance to ASTM standard D2584:

622       $V_f = (W_f \rho_m)/(W_f \rho_m + W_m \rho_f)$ (12)

623   where W_f is weight of αCell fibers which is 20%, W_m is the weight of polymer matrix which is

624   80%, ρ_f is the density of fibers ($\rho_f = 1.5$ g/cm^3),[49] and ρ_m is the density of matrix (ρ_m values of

625   PHB and PHBV are 1.18 and 1.10 g/cm^3, respectively). V_f values of PHB and PHBV based

626   composites were 16% and 15%, respectively.

627

628   3.3.7. Rheological analysis

629   The dynamic rheological measurements (G', G" and η*) were determined using a Bohlin

630   CVO 100 rheometer, parallel plate (25 mm Ø), in oscillating shear mode with an ETC module on

631   molded discs (2 mm x 25 mm Ø) samples. Experiments were performed in the linear viscoelastic

632   region. For PHB and PHBV based materials, measurements were carried out at 175 and 170 °C,

633   respectively, in the frequency range of 0.1 to 100 rad/s at an applied iso-strain of 0.5%. Data was

634   analyzed using the Bohlin rheology v6.51 software.

635

636   **4. Conclusion**

637   The use of DCP in grafting modification of αCell/PHB and αCell/PHBV biocomposites via

638   *in-situ* reactive extrusion process was successful to achieve beneficial properties. Surface

639   morphology by SEM revealed better compatibility of cellulose in the polymer (PHB and PHBV)

640   matrix of the resultant biocomposites due to grafting modification as compared to blends. The

641   tensile tests showed the grafting increased the toughness and flexibility of biocomposites due to

642   the enhanced fiber-polymer matrix interaction and lower degree of crystallinity as compared to

643   neat polymers and simple blends. The degree of crystallinity of the composites was reduced

644   through grafting, which was reflected by the crystallinity indices estimated from quantitative

645   FTIR and WAXD analyses. Grafting was found to have a significant influence on the thermal

646   properties (e.g. stability) of αCell-*g*-PHB/PHBV biocomposites. Lower processing temperatures

647   and shorter cycle times during melt processing could be achieved and further minimize

648   degradation. Grafting improved the interfacial bonding between αCell fibers and polymer matrix

649   as determined by the adhesion factor. It can be concluded that this approach afforded cellulose

650   reinforced bioplastic composite materials with significantly improved mechanical and thermal

651   properties by chemically grafting the fibers with the matrix to improve stress transfer. This

652   grafting modification was achieved via a one-step reactive extrusion process and can provide a

653   sustainable strategy to utilize cellulose fibers derived from various renewable resources

654   including any at-risk intermountain wood species to create value added products. This developed

655   technique can be applied to PHB/PHBV biosynthesized from waste substrate by mixed microbial

656   consortia to lower the cost of these materials which will help their applications as bulk materials.

Acknowledgement

660 supporting the DSC and DMA, and (iii) ThermoScientific for the FTIR spectrometer.

661 ## References

662 1. G.-Q. Chen and M. K. Patel, *Chem. Rev.*, 2012, **112**, 2082-2099.

663 2. R. U. Halden, *Annual Review of Public Health*, 2010, **31**, 179-194.

664 3. D. Garlotta, *J. Polym. Environ.*, 2001, **9**, 63-84.

665 4. T. Mekonnen, P. Mussone, H. Khalil and D. Bressler, *Journal of Materials Chemistry A*,
666 2013, **1**, 13379.

667 5. J. Lunt, *Polym. Degrad. Stab.*, 1998, **59**, 145-152.

668 6. M. Yamaguchi and K. Arakawa, *Eur. Polym. J.*, 2006, **42**, 1479-1486.

669 7. R. M. Rasal, A. V. Janorkar and D. E. Hirt, *Prog. Polym. Sci.*, 2010, **35**, 338-356.

670 8. A. Youngblood, J. Zhu and C. T. Scott, presented in part at the National Silviculture
671 Workshop, Boise, Idaho, 15–18 June, 2009.

672 9. L. Wei, A. G. McDonald, C. Freitag and J. J. Morrell, *Polym. Degrad. Stab.*, 2013, **98**,
673 1348-1361.

674 10. K. Suzuki, A. Sato, H. Okumura, T. Hashimoto, A. N. Nakagaito and H. Yano, *Cellulose*,
675 2013, **21**, 507-518.

676 11. C. Fonseca-Valero, A. Ochoa-Mendoza, J. Arranz-Andrés and C. González-Sánchez,
677 *Composites Part A*, 2015, **69**, 94-104.

678 12. M. Pöllänen, M. Suvanto and T. T. Pakkanen, *Compos. Sci. Technol.*, 2013, **76**, 21-28.

679 13. A. K. Bledzki and J. Gassan, *Prog. Polym. Sci.*, 1999, **24**, 221-274.

680 14. M. Bengtsson, P. Gatenholm and K. Oksman, *Compos. Sci. Technol.*, 2005, **65**, 1468-
681 1479.

682 15. L. C. Tomé, R. J. B. Pinto, E. Trovatti, C. S. R. Freire, A. J. D. Silvestre, C. P. Neto and
683 A. Gandini, *Green Chem.*, 2011, **13**, 419.

684 16. A. Gandini, *Green Chem.*, 2011, **13**, 1061.

685 17. O. Faruk, A. K. Bledzki, H.-P. Fink and M. Sain, *Prog. Polym. Sci.*, 2012, **37**, 1552-
686 1596.

687 18. M. John and S. Thomas, *Carbohydr. Polym.*, 2008, **71**, 343-364.

688   19.   D. Roy, M. Semsarilar, J. T. Guthrie and S. Perrier, *Chem. Soc. Rev.*, 2009, **38**, 2046-
689   2064.

690   20.   L. Yu, K. Dean and L. Li, *Prog. Polym. Sci.*, 2006, **31**, 576-602.

691   21.   S. A. Madbouly, J. A. Schrader, G. Srinivasan, K. Liu, K. G. McCabe, D. Grewell, W. R.
692   Graves and M. R. Kessler, *Green Chem.*, 2014, **16**, 1911.

693   22.   L. Wei, S. Liang and A. G. McDonald, *Ind. Crop. Prod.*, 2015, **69**, 91–103.

694   23.   D. Roy, M. Semsarilar, J. T. Guthrie and S. Perrier, *Chem. Soc. Rev.*, 2009, **38**, 2046-
695   2064.

696   24.   A. Carlmark, E. Larsson and E. Malmström, *Eur. Polym. J.*, 2012, **48**, 1646-1659.

697   25.   N. Le Moigne, M. Longerey, J.-M. Taulemesse, J.-C. Bénézet and A. Bergeret, *Ind.*
698   *Crop. Prod.*, 2014, **52**, 481-494.

699   26.   L. Wei, A. G. McDonald and N. M. Stark, *Biomacromolecules*, 2015, **16**, 1040–1049.

700   27.   T. A. Clark, K. L. Mackie, P. H. Dare and A. G. McDonald, *J. Wood Chem. Technol.*,
701   1989, **9**, 135-166.

702   28.   J. Yang, J.-J. Zhao, F. Xu and R.-C. Sun, *ACS Appl. Mater. Interfaces*, 2013, **5**, 12960-
703   12967.

704   29.   K. Joseph and S. Thomas, *Polymer*, 1996, **37**, 5139-5149.

705   30.   W. J. Orts, R. H. Marchessault, T. L. Bluhm and G. K. Hamer, *Macromolecules*, 1990,
706   **23**, 5368-5370.

707   31.   K. Sudesh, H. Abe and Y. Doi, *Prog. Polym. Sci.*, 2000, **25**, 1503-1555.

708   32.   L. Wei, N. M. Guho, E. R. Coats and A. G. McDonald, *J. Appl. Polym. Sci.*, 2014, **131,**
709   **40333, doi: 10.1002/app.40333**.

710   33.   D. Maldas and B. V. Kokta, *J. Adhes. Sci. Technol.*, 1994, **8**, 1439-1451.

711   34.   N. M. Barkoula, S. K. Garkhail and T. Peijs, *Ind. Crop. Prod.*, 2010, **31**, 34-42.

712   35.   M. Avella, G. La Rota, E. Martuscelli and M. Raimo, *J. Mater. Sci.*, 2000, **35**, 829-836.

713   36.   S. Modi, K. Koelling and Y. Vodovotz, *Eur. Polym. J.*, 2011, **47**, 179-186.

714   37.   L. Wei and A. G. McDonald, *J. Appl. Polym. Sci.*, 2015, **132, Doi: 10.1002/app.41724**.

715   38.   R. Bhardwaj, A. K. Mohanty, L. T. Drzal, F. Pourboghrat and M. Misra,
716   *Biomacromolecules*, 2006, **7**, 2044-2051.

717 39. M. Scandola, M. L. Focarete, G. Adamus, W. Sikorska, I. Baranowska, S. Swierczek, M.
718 Gnatowski, M. Kowalczuk and Z. Jedlinski, *Macromolecules*, 1997, **30**, 2568-2574.

719 40. J. O. Zoppe, M. S. Peresin, Y. Habibi, R. A. Venditti and O. J. Rojas, *ACS Appl. Mater.*
720 *Interfaces*, 2009, **1**, 1996-2004.

721 41. E. Ten, D. F. Bahr, B. Li, L. Jiang and M. P. Wolcott, *Ind. Eng. Chem. Res.*, 2012, **51**,
722 2941-2951.

723 42. D. Yan, W.-J. Wang and S. Zhu, *Polymer*, 1999, **40**, 1737-1744.

724 43. D. H. S. Ramkumar and M. Bhatacharya, *Polym. Eng. Sci.*, 1998, **38**, 1426-1435.

725 44. J. S. Fabiyi, A. G. McDonald, M. P. Wolcott and P. R. Griffiths, *Polym. Degrad. Stab.*,
726 2008, **93**, 1405-1414.

727 45. S. Liang and A. G. McDonald, *J. Agric. Food Chem.*, 2014, 140805102128006.

728 46. L. E. Alexander, *X-ray diffraction method in polymer science*, Wiley-Interscience, New
729 York, 1969.

730 47. P. J. Barham, A. Keller and E. L. Otun, *J. Mater. Sci.*, 1984, **19**, 2781-2794.

731 48. J. Kubát, M. Rigdahl and M. Welander, *J. Appl. Polym. Sci.*, 1990, **39**, 1527–1539.

732 49. W. A. Sisson, in *Cellulose and cellulose derivatives*, ed. E. Ott, Interscience, New York.,
733 1943, ch. 4, pp. 214, vol. 5, ch. 3.

734

735

736

737   **Table 1** Chemical composition of the lodgepole pine wood and isolated αCell fibers (dry basis).

Composition	Lodgepole pine wood (%)	α-Cellulose (%)
Cellulose	39.1	95.9
Glucan 6C	39.1	95.9
Hemicellulose	33.1	3.9
Xylan 5C	5.3	3.8
Galactan 6C	11.5	0.0
Mannan 6C	16.3	0.1
Arabinan 5C	1.5	0.0
Lignin	26.9	0.2
Klason lignin	26.5	0.2
Acid soluble lignin (ASL)	0.4	0.0
CH_2Cl_2 extractives	1.7	0.0
Ash	0.01	0.0

738

739 **Table 2** Yield of each fraction of αCell fibers retained on sieves with various openings, and the

740 averaged fiber length, diameter, and the aspect ratio measured by microscopic analysis.

Retained on mesh	Sieve opening (μm)	Particle weight fraction (%)	Fiber length (L, mm)[b]	Fiber diameter (d, μm)[a]	Aspect ratio (L/d)
40	420	7.3	-	-	-
60	250	6.3	-	-	-
80	177	16.0	0.8 ± 0.1	19.0 ± 1.6	42.1
100	149	11.4	0.7 ± 0.1	18.7 ± 2.8	37.4
200	70	37.5	0.6 ± 0.1	18.5 ± 2.0	32.4
< 200	<70	21.5	0.4 ± 0.1	14.0 ± 2.1	28.6
Average			0.5	15.1	29.3

741 [a] The fiber length and diameter of αCell fibers of the 60 and 40 mesh fractions could not be

742 accurately determined due to fiber bundles as shown in Fig. 2a and 2b.

743

744   **Table 3** Crystallinity parameters characterized by FTIR and WAXD. [a]

Sample	FTIR			WAXD			
	$TCI_{\alpha Cell}$	$I_{C=O, PHB/PHBV}$	$I_{C-O, PHB/PHBV}$	$CrI\%_{\alpha Cell}$	$CrI\%_{PHB/PHBV}$	D (002) (Å)	D (020) (Å)
αCell	0.4	-	-	59.1	-	250	-
PHB	-	3.8	2.0	-	61.0	-	1274
αCell-PHB	0.3	3.3	0.6	56.4	57.9	233	1108
αCell-*g*-PHB	0.1	2.2	0.4	33.9	45.4	90	312
PHBV	-	2.7	0.8	-	36.2	90	190
αCell-PHBV	0.3	2.6	0.4	40.2	34.2	82	153
αCell-*g*-PHBV	0.1	1.8	0.1	28.7	26.4	40	97

745   [a] Crystal sizes were determined in the direction perpendicular to the planes of (002) and (020) for

746   αCell and polymers PHB and PHBV, respectively.

747 **Table 4** Density (ρ), tensile strength (σ), tensile (Young's) modulus (E), elongation at break (ε),

748 and energy at break (EAB) of molded neat PHB/PHBV and their biocomposites samples (10

749 replicates). Standard deviation values are given in parentheses. Samples with same letter are not

750 significantly different at 95% confidence interval of probability using Tukey's paired t-tests.

Sample	ρ (g/cm^3)	E (GPa)	σ (MPa)	ε (%)	EAB (J)
Neat PHB	1.18 (0.02)[abc]	2.2 (0.3)[a]	23.1 (3.3)[a]	13.6 (1.0)[a]	0.33 (0.03)[a]
αCell-PHB	1.14 (0.03)[abc]	2.6 (0.2)[ab]	25.9 (1.4)[ab]	11.2 (0.3)[b]	0.41 (0.03)[b]
αCell-g-PHB	1.10 (0.02)[abc]	5.5 (0.7)[c]	28.1 (1.8)[c]	13.2 (2.0)[ac]	0.60 (0.05)[c]
Neat PHBV	1.18 (0.01)[def]	0.9 (0.1)[d]	11.8 (2.0)[d]	19.6 (1.8)[d]	0.45 (0.03)[d]
αCell-PHBV	1.10 (0.02)[def]	1.3 (0.1)[e]	13.9 (2.5)[e]	15.4 (1.8)[e]	0.53 (0.05)[e]
αCell-g-PHBV	1.06 (0.02)[def]	2.4 (0.3)[f]	15.9 (1.7)[f]	18.8 (1.0)[df]	0.76 (0.05)[f]

751

752

753 **Table 5** Thermal degradation temperatures of PHB and PHBV based biocomposites obtained

754 from TGA data. [a]

Samples	T_{onset} (°C)	T_{max} (°C)		T_{comp} (°C)
		T_{PHB}/T_{PHBV} (°C)	$T_{\alpha Cell}$ (°C)	
α-Cellulose	303		342	400
PHB	263	285		303
αCell-PHB	264	287	328	358
αCell-g-PHB	277	298	335	364
PHBV	250	270		292
αCell-PHBV	253	273	334	362
αCell-g-PHBV	260	284	340	363

755 [a] T_{onset} = beginning weight loss; T_{max} = the temperature of maximum decomposition rate; T_{PHB},

756 T_{PHBV} = maximum decomposition rate of PHB and PHBV degradation stage (the 1st stage of

757 biocomposites), respectively; $T_{\alpha Cell}$ = maximum decomposition rate of αCell degradation (the 2nd

758 stage of biocomposites); T_{comp} = 100% mass loss onset point.

759

760 **Table 6** Crystallization temperature (T_c), peak temperatures of the low- and high-temperature

761 endotherms (T_{m1} and T_{m2}), and degree of crystallinity (X_c %). Standard deviation values are

762 given in parentheses.

Samples	T_g (˚C)	T_{m1}(˚C)	T_{m2} (˚C)	X_c (%)	T_c (˚C)	T_c (˚C)	ΔH_c (J/g)
Neat PHB	4.9	159	169	53.4 (1.2)	85	ND	67
αCell-PHB	5.3	161	171	50.0 (0.5)	121	ND	63
αCell-*g*-PHB	6.9	155	164	43.0 (2.3)	103	ND	55
Neat PHBV	-4.0	129	153	17.8 (0.5)	67	ND	27
αCell-PHBV	-2.0	126	151	16.8 (1.1)	39	56.4	22
αCell-*g*-PHBV	-0.5	118	135	4.60 (0.2)	ND	76.5	ND

763 ND: not detected.

764

765   **Table 7** Comparative storage moduli (E') at selected temperatures, tanδ and adhesion factor (A)

766   near to room temperature (30 ˚C) of neat PHB and PHBV based samples. Standard deviation

767   values are given in parentheses.

Samples	Storage modulus E' (MPa)			Tanδ			V_f(%)	$A_{30°C}$
	30 ˚C	50 ˚C	70 ˚C	Tan$\delta_{30\,°C}$	Tan$\delta_{50\,°C}$	Tan$\delta_{70\,°C}$		
Neat PHB	1797	1466	1276	0.076	0.037	0.040	0	-
αCell-PHB	2395	2073	1820	0.070	0.043	0.050	16 (0.5)	1.25 (0.20)
αCell-g-PHB	2869	2255	1934	0.040	0.035	0.054	15 (1.2)	0.28 (0.00)
Neat PHBV	630	548	439	0.090	0.065	0.074	0	-
αCell-PHBV	1182	742	486	0.065	0.068	0.090	16 (0.5)	0.72 (0.14)
αCell-g-PHBV	1432	985	706	0.050	0.080	0.104	15 (1.2)	0.32 (0.02)

768   Note: the differences of moduli and Tanδ between duplicates were less than 20 MPa and 0.005,

769   respectively; hence standard deviation was not reported.

770
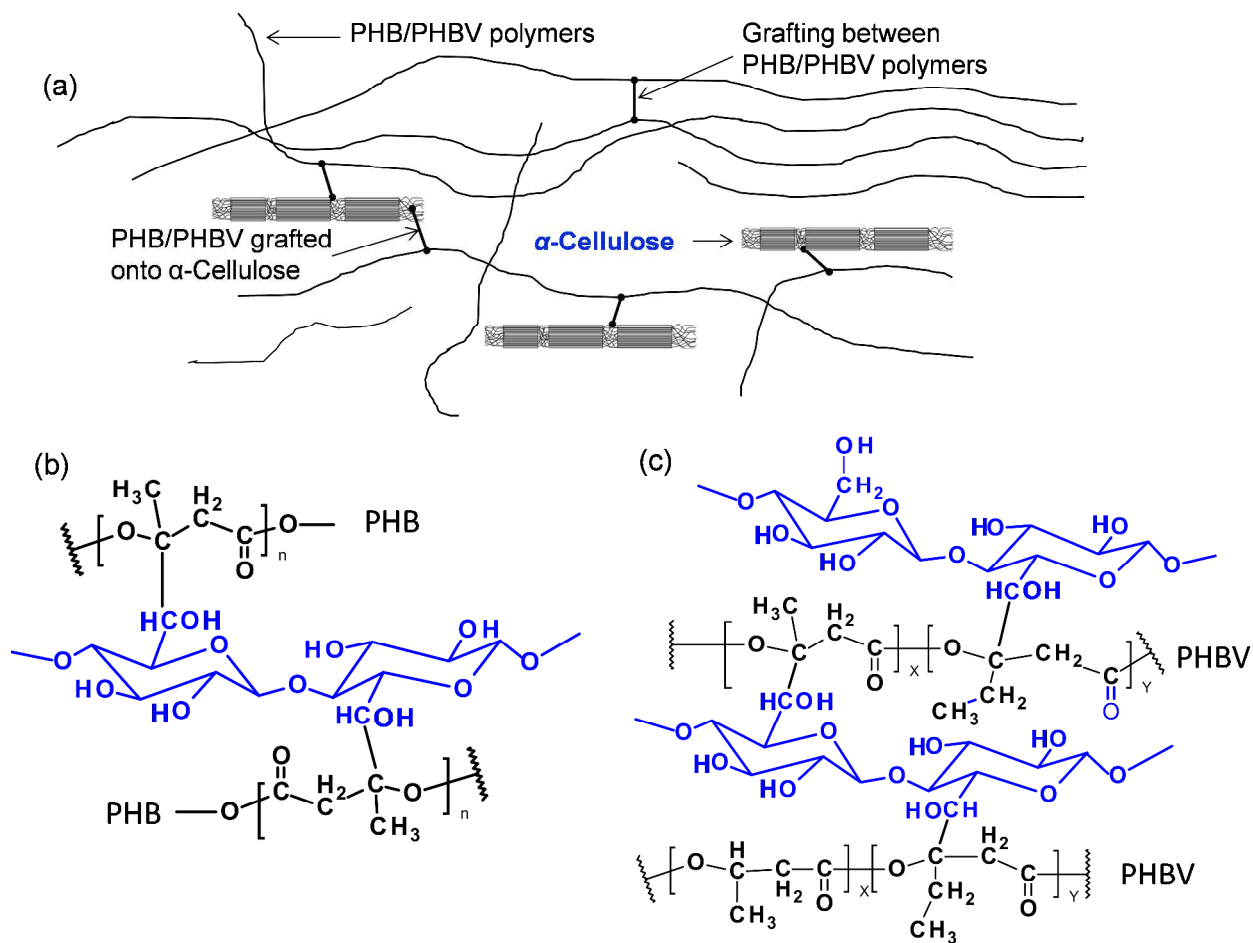
Fig. 1. Generalized schematic representation of grafted PHB or PHBV polymers onto αCell (a),

and the chemical structures of grafted αCell-*g*-PHB (b) and αCell-*g*-PHBV (c) biocomposites.

773

774
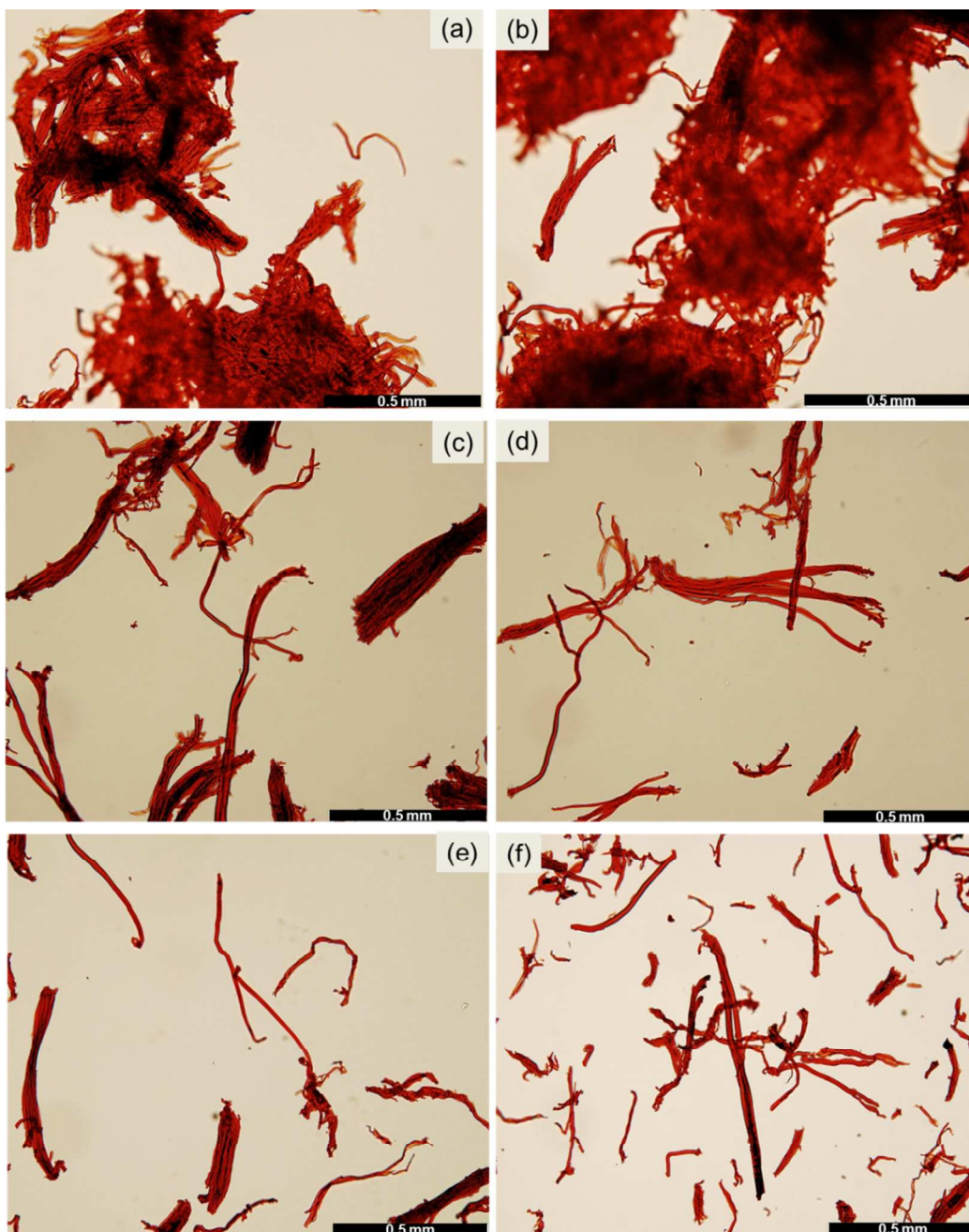
Fig. 2 Optical micrographs of αCell fibers fractions classified (a) >40 mesh, (b) >60 mesh,

776 (c) >80 mesh, (d) >100 mesh, (e) >200 mesh and (d) <200 mesh.

777
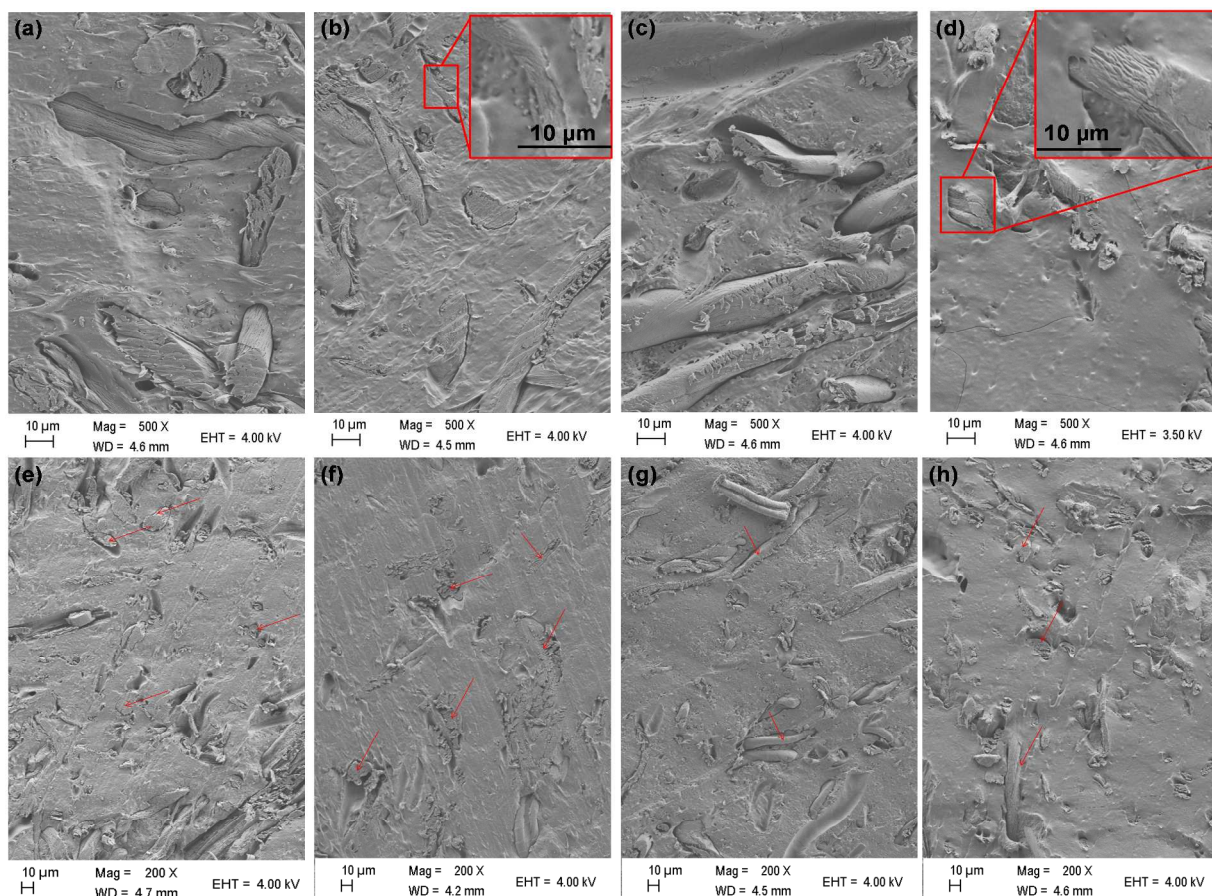
Fig. 3 SEM micrographs of surface morphologies of αCell-PHB (a: 500x; e: 200x), αCell-*g*-PHB (b: 500x; f: 200x), αCell-PHBV (c: 500x; g: 200x), and αCell-*g*-PHBV (d: 500x; h: 200x) composites. Note: fiber and polymer matrix interface was shown in in-set micrographs with larger magnification (1000x) of the grafted composites (b and d); fibers are pointed out by arrows.

786
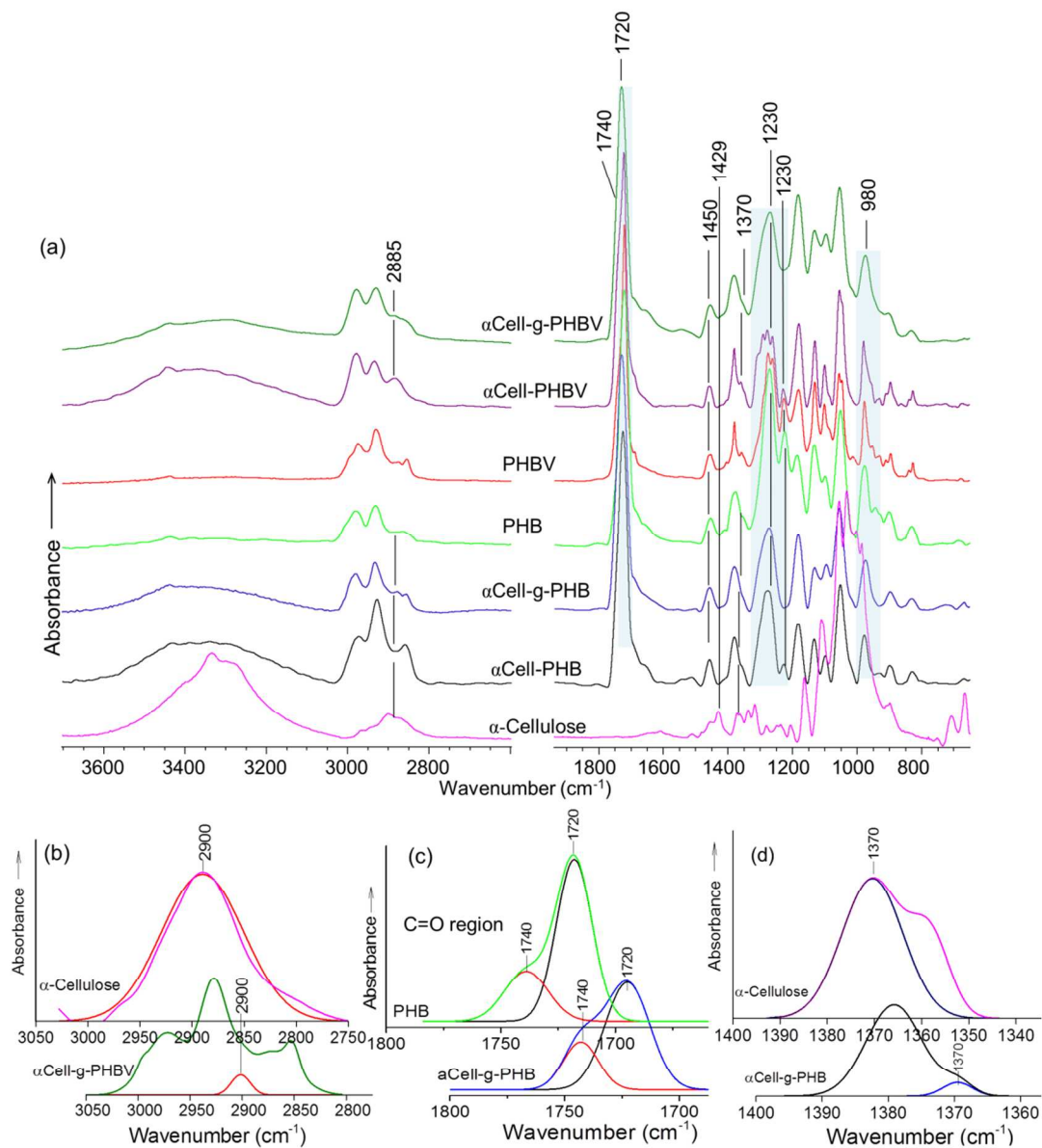
Fig. 4 (a) FTIR spectra for α-cellulose, PHB, PHBV, and their composites samples; (b) $-C-H$

stretching (2900 cm^{-1}) fitted bands for αCell and αCell-g-PHBV composites; (c) carbonyl (C=O)

fitted peaks for PHB and αCell-g-PHB composite, and (d) $-C-H$ bending (1370 cm^{-1}) fitted
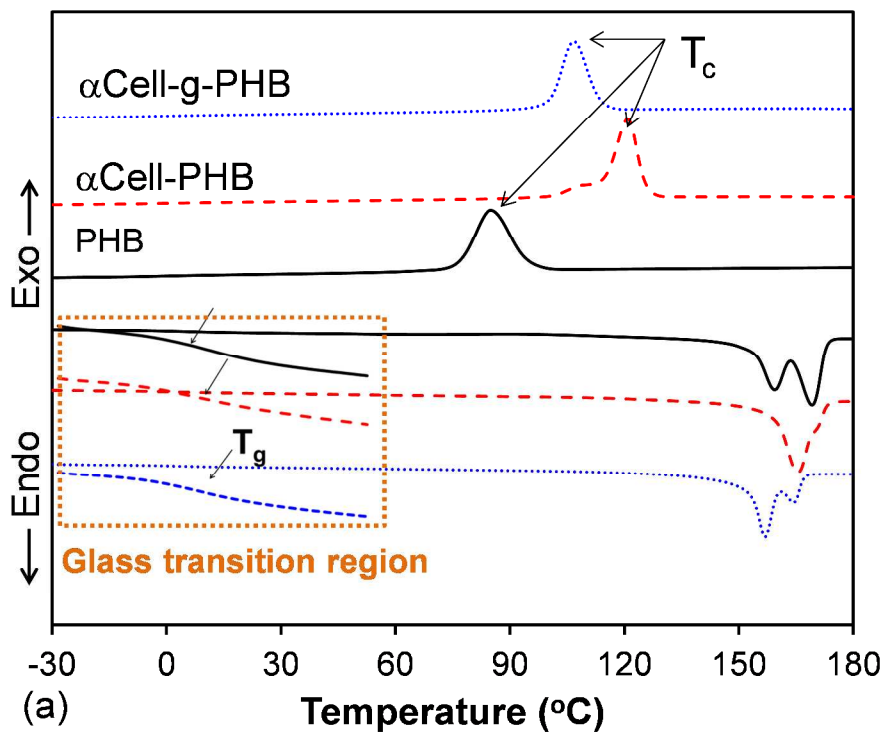
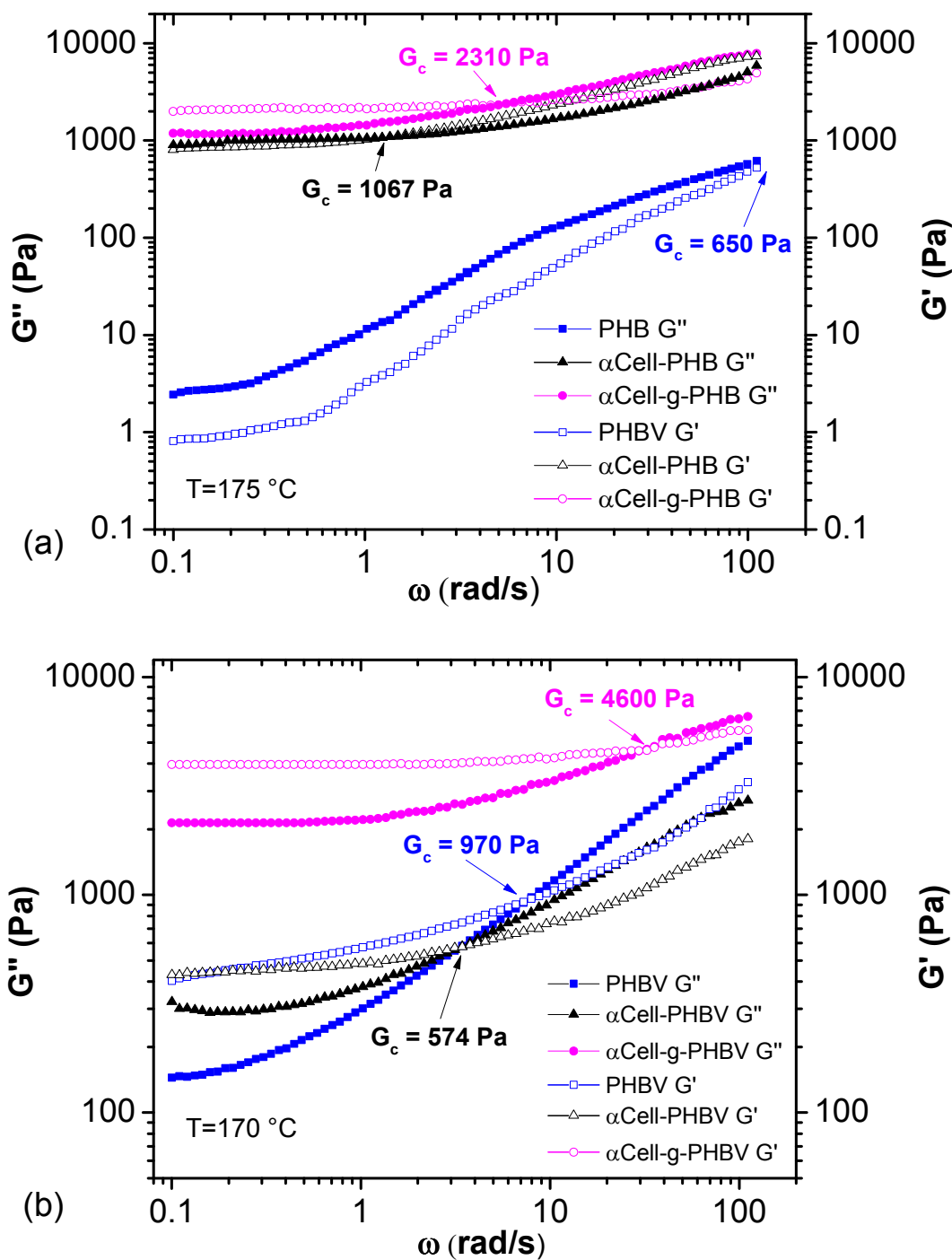peaks for αCell and αCell-g-PHB composite.

791
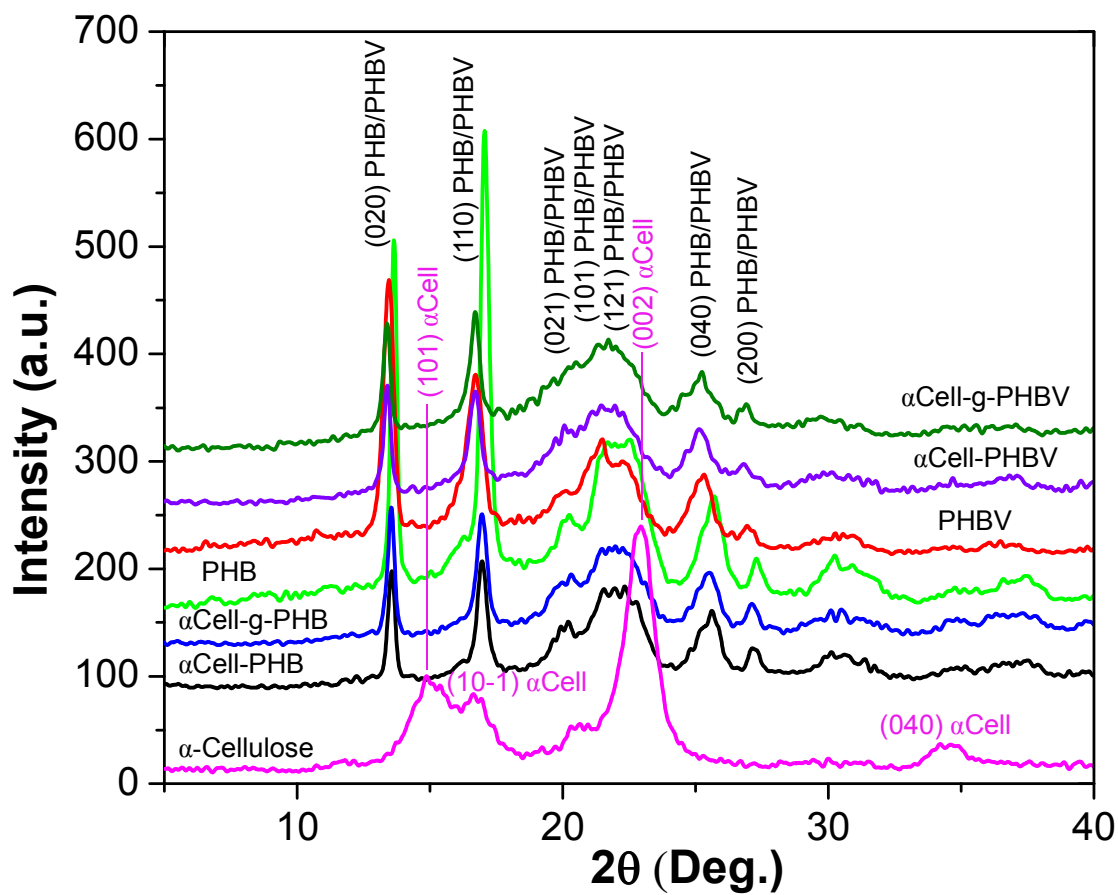
792

793 **Fig. 5** XRD diffractograms of *α*Cell, PHB, PHBV, blended composite (*α*Cell-PHB and *α*Cell-

794 PHBV) and grafted composite (*α*Cell-*g*-PHB and *α*Cell-*g*-PHBV) samples.

795
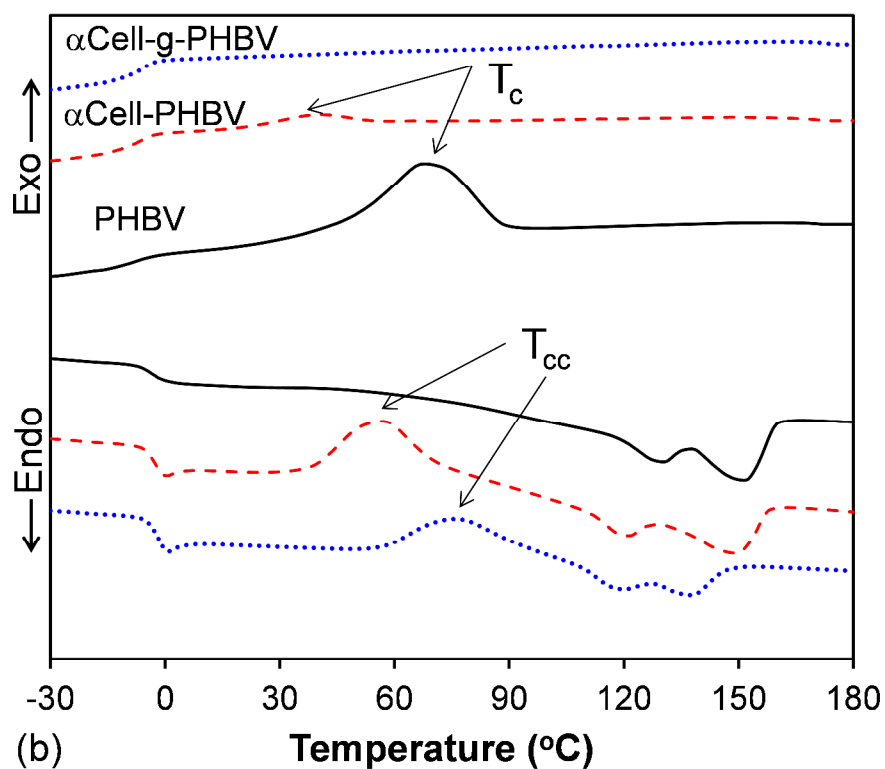
Fig. 6 DSC cooling and the 2nd heating curves of (a) PHB, αCell-PHB and αCell-*g*-PHB and (b) PHBV, αCell-PHBV and αCell-*g*-PHBV samples.

Fig. 7 Effect of grafting on dynamic rheology storage (G') and loss (G") moduli of (a) PHB, αCell-PHB, and αCell-g-PHB samples at 175 °C and (b) PHBV, αCell-PHBV and αCell-g-PHBV samples at 170 °C. G_c is the crossover modulus when G' = G".
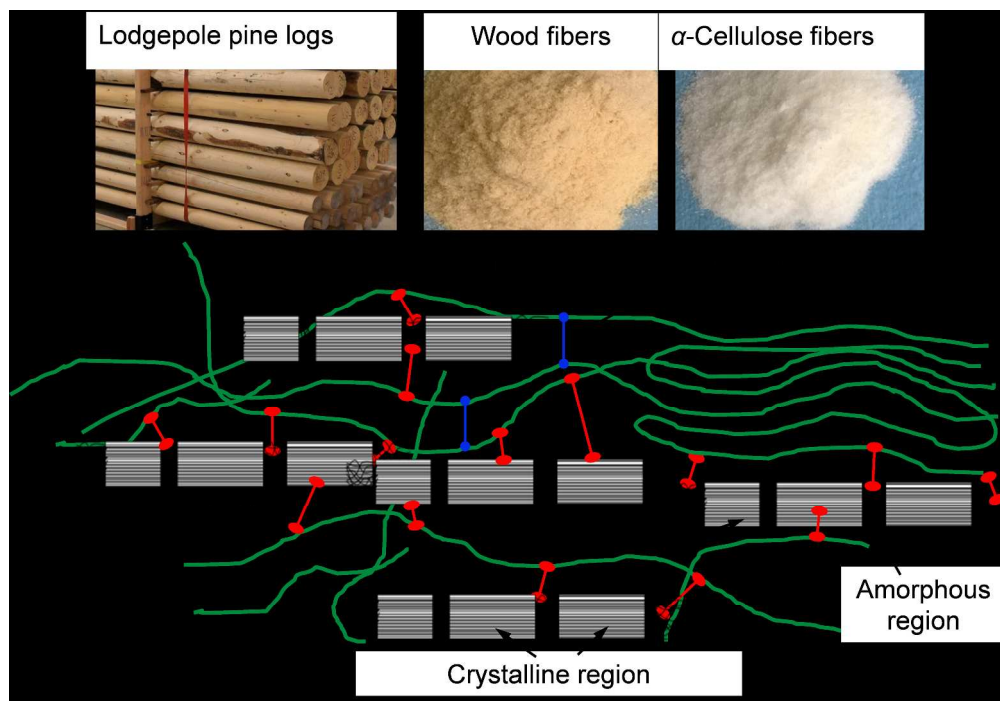
This in-situ grafting modification offers an effective approach to improve the properties of the biocomposite materials from sustainable resources

1339x929mm (96 x 96 DPI)